De Baere, I., Van Paepegem, W. and Degrieck, J. (2008). On the feasibility of a three-point bending setup for the validation of (fatigue) damage models for thin composite laminates. Polymer Composites, 29(10), 1067-1076

On the feasibility of a three-point bending setup for the validation of (fatigue) damage models for thin composite laminates

I De Baere, W Van Paepegem and J Degrieck
Department of Mechanical Construction and Production, Faculty of Engineering, Ghent University. Sint-Pietersnieuwstraat 41, B-9000 Gent, Belgium.

E-mail: Ives.DeBaere@UGent.be

Abstract
After developing a damage model, validation of this model is a necessity. This validation should preferably be done under loading conditions which are different from the ones used for the development of the model.
This study investigates whether a three-point bending setup is suited for the validation of fatigue material models for thin fibre-reinforced composites with a low bending stiffness, developed in uni-axial loading conditions. First, the three-point bending setup, which can be used for both single-sided and fully reversed loading, is discussed. Then, some results of experiments are presented. This is followed by the numerical modelling of the bending setup.
It may be concluded that the three-point bending setup, although its very interesting loading conditions, is not ideally suited for model validation, due to the complicated and time-consuming numerical simulation.
The material used for this study was a carbon fabric-reinforced polyphenylene sulphide.

1. Introduction and Principle

The vast majority of fatigue tests on fibre-reinforced composites is performed in uni-axial tension/tension or tension/compression fatigue [1][2][3][4][5]. These tests are accepted by international standards (ASTM D3479) and provide the S-N data for the tested material.
Although bending fatigue tests are not widely accepted as a standard, they are used a lot for research purposes [6][7][8]. They do have some important advantages as well: (i) bending loads often occur in in-service loading conditions, (ii) there are no problems with buckling, compared to tension/compression fatigue, and (iii) the required forces are much smaller. To evaluate the stiffness degradation and damage growth in the fibre-reinforced laminate, the hysteresis loop of one loading cycle can be measured. In case of three-point bending fatigue, the history of bending force versus midspan displacement is recorded.
This study investigates whether the three-point bending setup with fully reversed loading can be used for the validation of (a combination of) damage models for thin composite laminates in static or fatigue loading conditions.
In the following paragraph, the used material and equipment is discussed. Extra attention is given to the three-point bending setup with rotational supports, which can be used for fully reversed loading. This is followed by an overview of all bending experiments performed. Then, the modelling of the bending setup is discussed and finally, some conclusions are drawn.

2. Materials and Methods

2.1. Composite Material

The material under study was a carbon fibre-reinforced polyphenylene sulphide (PPS), called CETEX. This material is supplied to us by Ten Cate. The fibre type is the carbon fibre T300J 3K and the weaving pattern is a 5-harness satin weave with a mass per surface unit of 286 g/m^2. The 5-harness satin weave is a fabric with high strength in both directions and excellent bending properties.
The carbon PPS plates were hot pressed, only one stacking sequence was used for this study, namely a $[(0°,90°)]_{4s}$ were (0º,90º) represents one layer of fabric.
The in-plane elastic properties of the individual carbon PPS lamina were determined by the dynamic modulus identification method as described in [9] and are listed in Table 1.

Table 1 In-plane elastic properties of the individual carbon/PPS lamina (dynamic modulus identification method).

E_{11}	56.0	GPa
E_{22}	57.0	GPa
ν_{12}	0.033	-
G_{12}	4.175	GPa

The tensile strength properties were supplied by Ten Cate Advanced Composites and are listed in Table 2.

Table 2 Tensile strength properties of the individual carbon/PPS lamina (Supplied by Ten Cate AC).

X_T	765.0	MPa
ε_{11}^{ult}	0.011	-
Y_T	754.0	MPa
ε_{22}^{ult}	0.013	-
S_T	110.0	MPa

The test coupons were sawn with a water-cooled diamond saw. The dimensions of the coupons used for the bending experiments are shown in Figure 1, all dimensions are in millimetres.

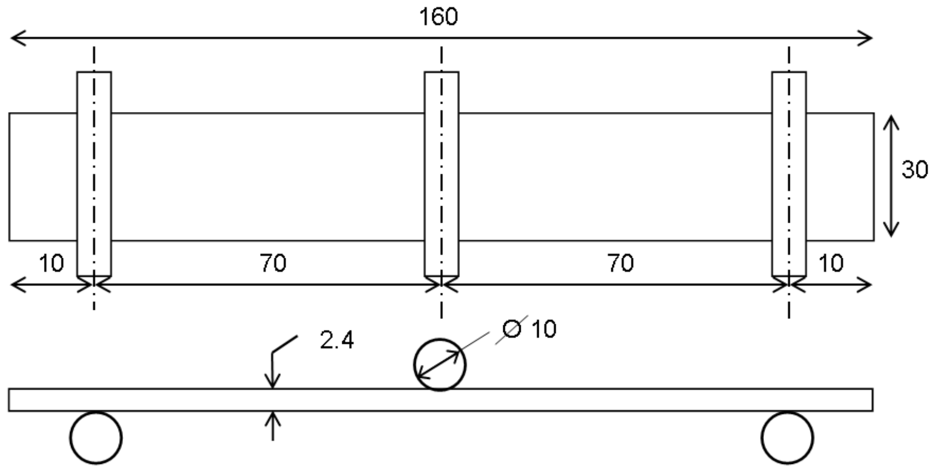

Figure 1 Dimensions of the used bending coupon in millimetres.

2.2. Three-point bending setup with rotating supports

2.2.1. Introduction

The loading conditions in a three-point bending setup are interesting for the validation of damage models. Figure 2 shows the resulting transverse force and bending moment in a beam, subjected to three-point bending. For an isotropic material, this bending moment results in the following stresses [10]:

$$\sigma_{xx} = \frac{Mz}{I_{yy}} \tag{1}$$

Where I_{yy} is the moment of inertia of the cross section of the beam and z is the position in the beam with respect to the neutral fibre. This means that the upper side of the beam is loaded in compression and the lower side in tension, with a maximum absolute value of:

$$\sigma_{xx,MAX} = \left| \frac{M_{MAX} \frac{h}{2}}{I_{yy}} \right| \tag{2}$$

With h being the total height of the beam and M_{MAX} the maximum bending moment in the centre of the beam. The latter is equal to FL/4 as is shown in Figure 2.

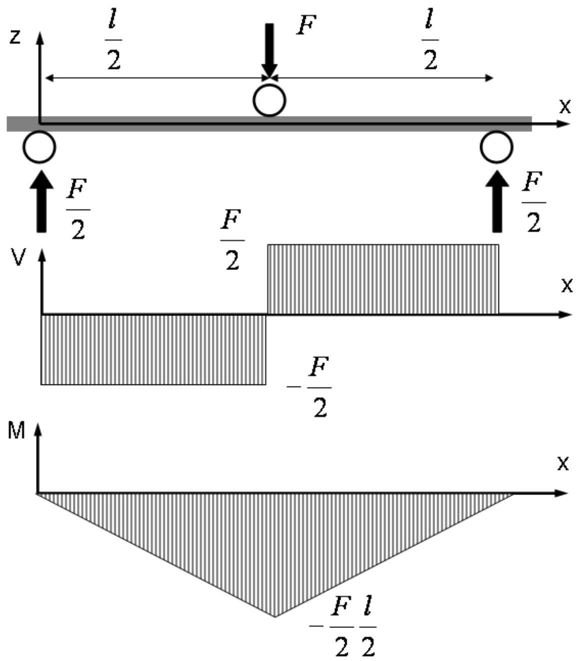

Figure 2 Transverse force and bending moment in a three-point bending setup.

Therefore, this loading setup already imposes both tension and compression in the specimen, but at different locations. This setup could be used for the validation of i) a static damage model that implicates both tensile and compressive damage; ii) a combination of a tension-tension and a compression-compression fatigue damage model.

When single-sided bending is used (see Figure 3), the deflection of the centre of the specimen evolves between zero and a certain value u_{max} (displacement controlled).

Figure 3 Single-sided three-point bending test.

This value of u_{max} may be very large for thin composites with low bending stiffness, 20 mm was reached for the $[0°,90°)]_{4s}$ carbon fabric-PPS in Figure 3. Another problem that occurs at large midspan displacements, is that the friction on the outer supports influences the shape of the hysteresis loops, as has been reported in [11].

In fatigue testing, depending on the stacking sequence, the specimens can show permanent deflection after a few thousands of cycles. When performing a displacement controlled test, the latter results in the loss of contact of the indenter when its displacement is smaller than the permanent deflection. In the next cycle, the indenter impacts on the surface of the specimen, causing impact damage and as a result, the fatigue data is corrupted.

This problem can be solved if the permanent deflection is kept symmetrically, which means it is kept at zero deflection. This can easily be obtained by fully reversed bending, where the displacement of the indenter varies between $-u_{max}$ and $+ u_{max}$.

If the test is performed in load control, then this 'loss of contact' problem does not occur. However, a load controlled bending test requires a very accurate PID controller and the test should be performed at lower frequencies than under displacement control. Furthermore, the load controlled simulation resulted in a lot more convergence problems. Therefore, load control has not been considered here.
When fully reversed bending is used, each side of the specimen is successively loaded in tension as well as in compression. As a result, the material in the beam sees alternating tension and compression, which makes this setup ideal for the validation of tension-compression fatigue models.

2.2.1. Design

If fully reversed bending is considered, some changes must be made to the original setup as illustrated in Figure 3: i) for the central indenter as well as the outer supports, two contact cylinders are required, one for the upward and one for the downward motion. Since the centre of the specimen remains horizontal (see Figure 3, the right), no additional modifications are needed for the central indenter; ii) because the specimen rotates at its ends (see Figure 3, the right), the outer supports need to allow for this rotation. Otherwise, this would induce unwanted reaction forces in the specimen, corrupting the fatigue data. The used supports and indenter are shown in Figure 4 and the total setup in Figure 5.

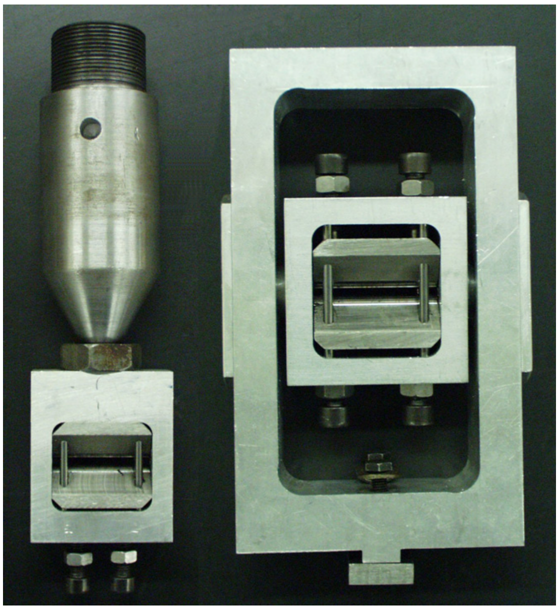

Figure 4 The rotating outer support (right) and the central roll (left).

Figure 5 The fully reversed three-point bending setup.

Details and drawings of this setup can be found in [12]. Figure 6 illustrates the described setup at maximum deflection, the rotation of the supports can be seen.

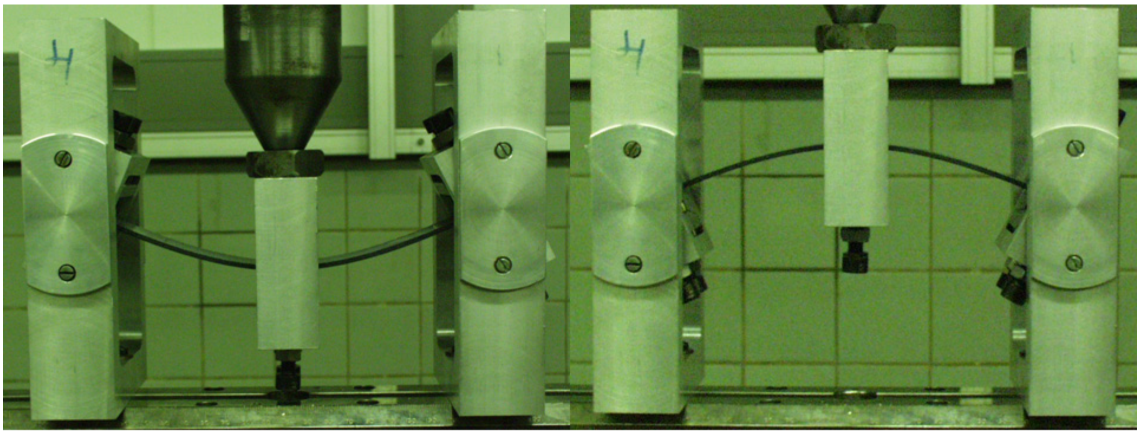

-20 mm deflection +20 mm deflection

Figure 6 Illustration of the fully reversed three-point bending with the described setup.

A problem that occurred during fatigue testing was the drifting of the specimen in the clamps. Tightening the outer supports is not an option, since this would induce membrane stresses in the specimen. Tightening the centre rolls may not be done either, because this pressure compresses the specimen through the thickness and makes the propagation of cracks more difficult. This corrupts the lifetime of the specimen.

To prevent the drifting of the specimen, a small U shaped object was mounted on the side of the outer support as illustrated in Figure 7. When the specimen is mounted, the supporting rolls should make contact without applying any extra pressure.

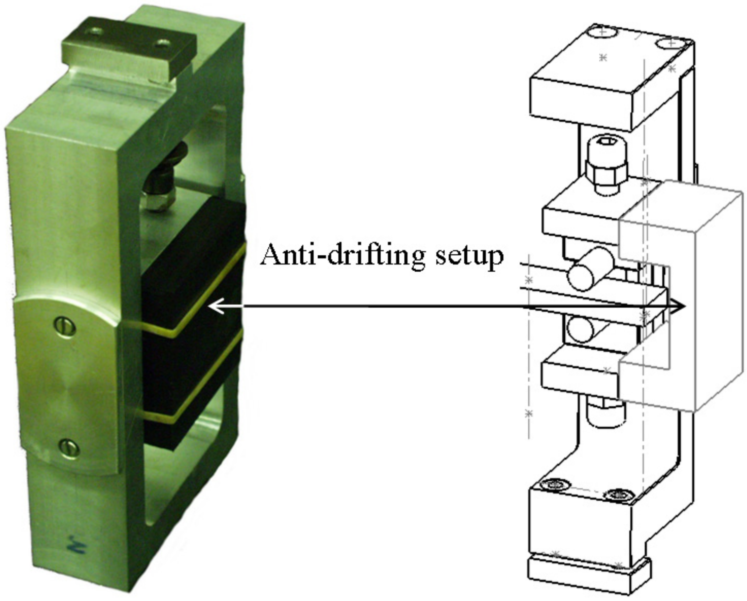

Figure 7 The anti-drifting setup.

2.3. Equipment

All bending tests were performed on a servo hydraulic INSTRON 1342 tensile testing machine with a FastTrack 8800 digital controller. The quasi-static bending tests were displacement-controlled with speeds of 2, 2400, 4800 and 7200 mm/min.

For the registration of the data, a combination of a National Instruments DAQpad 6052E for fireWire, IEEE 1394 and the SCB-68 pin shielded connecter were used. The load and displacement, given by the FastTrack controller, were sampled on the same time basis.

3. Experiments and Discussion

3.1.1. Testing Speeds

The preliminary static tests were done at different speeds, to verify whether the loading velocity has any influence on the bending stiffness and strength.

The first speed selected is 2 mm/min, for a quasi-static test. The other speeds are chosen with the fatigue tests in mind (Figure 8).

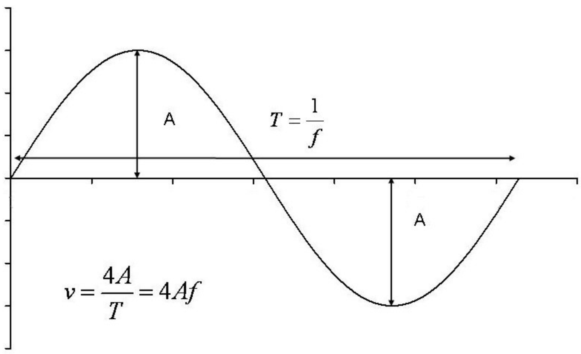

Figure 8 Determination of the displacement speed in a fatigue test.

A fatigue test with a displacement-amplitude of 7.5 mm (total displacement 15 mm) and a frequency of 0.5 Hz means a speed of 15 mm/s or 1200 mm/min. Given the same amplitude, but at a frequency of 2.5 Hz results in a speed of 75 mm/s or 4500 mm/min.

Taking the limits of the machine into account, speeds of 2400 mm/min and 4500 mm/min (= 75 mm/s) are chosen to characterise the material at deformation speeds that occur during fatigue testing. Since the interval between 2 mm/min and 2400 mm/min is quite large, a fourth speed of 300 mm/min is chosen.
Figure 9 shows the results of a few bending experiments at the mentioned speeds, performed on the setup with the rotating outer supports. It must be noted that the speed has no influence on the bending stiffness, or on the ultimate bending force. The small deviation in ultimate force is due to scatter in the results. All the specimens break at approximately 20 mm displacement at a corresponding force of approximately 900 N.

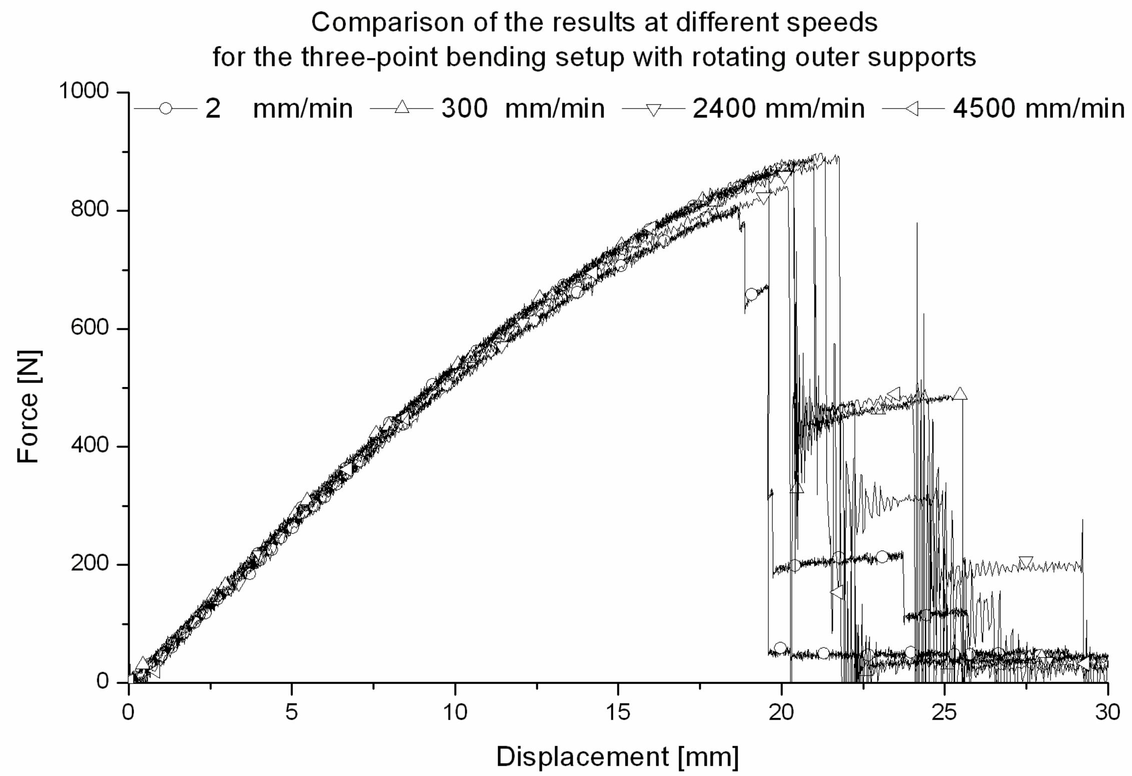

Figure 9 Force as a function of the displacement at different speeds.

However, there is a difference in the results for the single-sided bending setup with rigid supports (3ROLL) and the bending setup with rotating supports (6ROLL), as is illustrated in Figure 10. It can clearly be seen that for an equal displacement, the force is lower if the rotating outer supports are used. The bending stiffness and ultimate bending force are higher when the single-sided setup without rotating supports is used. This effect is entirely due to the setup, as will be proven in the next section, where the finite element modelling of the setup is discussed.
It may be noticed that for the bending setup with the rigid supports, the influence of the speed on bending stiffness and ultimate bending force is also negligible.

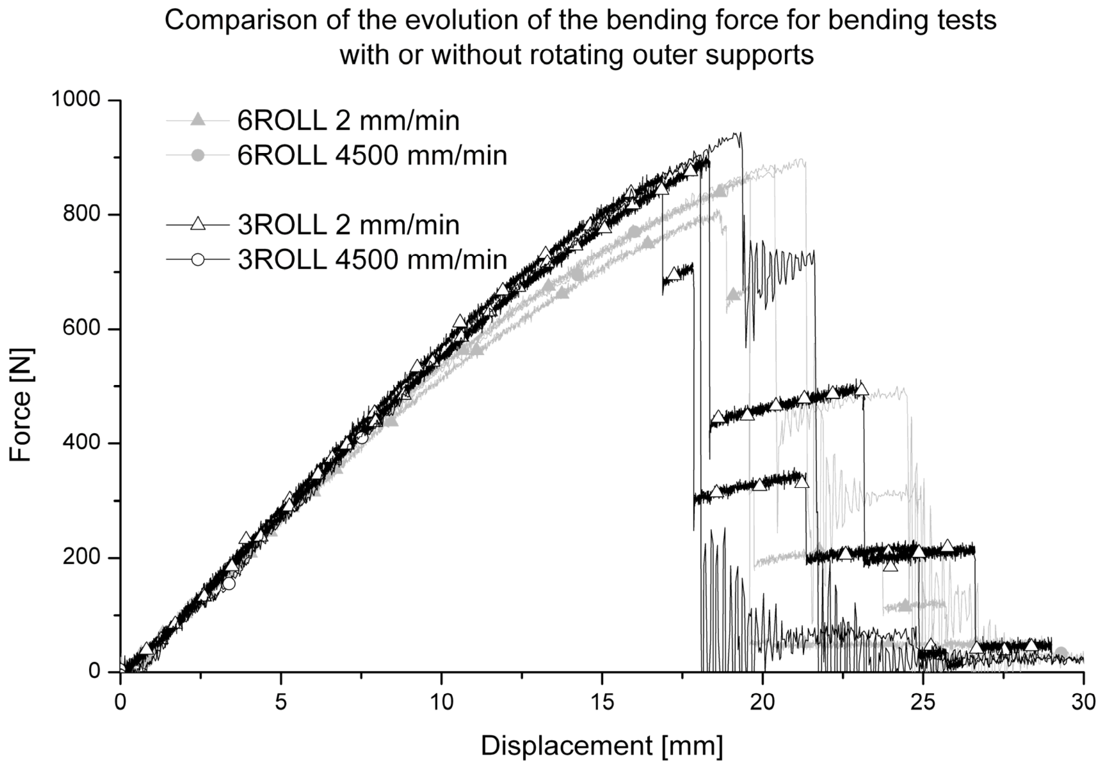

Figure 10 Illustration of the influence of the rotating outer supports in three point bending.

4. Finite element simulations

4.1. General

The used finite element software was ABAQUS™ Standard 6.4. As was mentioned in the previous paragraph, the speed does not have any significant influence on bending stiffness or ultimate force. As such, there is no need to use an explicit numerical solver and an implicit analysis was used. The computer on which all calculations were done was a Dell Inspiron 8200 with a Mobile Intel® Pentium® 4-m CPU with a clock frequency of 2.00 GHz and 1.00 Gb of RAM.

The modelling of the three-point bending setup in general has some difficulties. Figure 2 illustrates the loading conditions in a beam that is subjected to three-point bending. As can be seen, there is a transverse force V, equal to half of the loading force F, over the entire beam and the bending moment grows linearly until the centre of the beam.

These loading conditions cannot be modelled by equivalent loads and boundary conditions, which means that the rotating supports need to be modelled. The latter requires contact conditions with friction, which has its effect on the calculation time. A friction coefficient for friction between the carbon reinforced PPS, and steel was determined in [13]. If friction is omitted, then the force will be underestimated, because the resultant of the friction on the supports is not taken into account. Furthermore, the influence of the friction on the hysteresis loops, which is well proven in [11] is neglected. Furthermore, because of the large deformations, a geometrically nonlinear analysis must be performed.

In the following paragraphs, the modelling of the single-sided and fully reversed setup is discussed.

4.2. Single-sided three-point bending with rigid supports

In order to save calculation time, symmetry is used to model the setup, so only a quarter of the setup is implemented. This is illustrated in Figure 11.

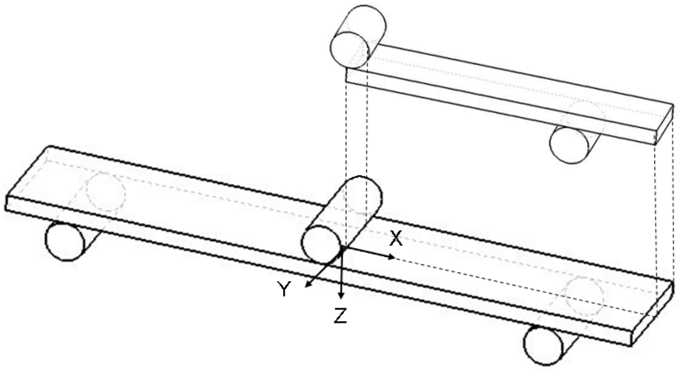

Figure 11 Modelling only a quarter of the total setup.

The dimensions of the modelled specimen are 2.4 mm x 15 mm x 80 mm and the rolls have a diameter of 10 mm and a length of 20 mm. The specimen is partitioned eight times, each partition representing one layer. Three more partitions are made for the contact surfaces. The rolls are also partitioned for a better mesh. The boundary conditions as well as the used mesh are illustrated in Figure 12.

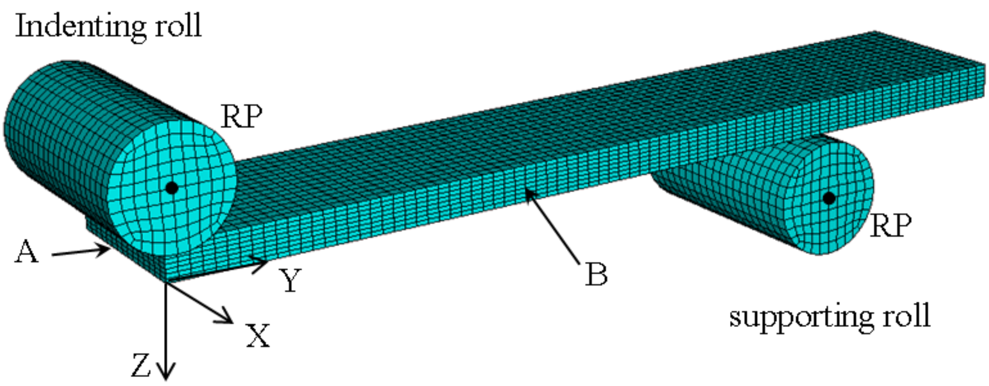

Figure 12 Illustration of the mesh and the boundary conditions for the three-point bending setup with rigid supports.

To model symmetry, the following boundary conditions are applied.
On plane A: $U_y = UR_x = UR_z = 0$.
On plane B: $U_x = UR_y = UR_z = 0$.
The reference point of the supporting role is completely fixed. For the indenting roll, the movement along the x-axis and y-axis is inhibited and a displacement of 20 mm is imposed on the reference point in the case of a displacement controlled test.

For the specimen, a quadratic brick element with reduced integration, C3D20R, is used. For the material, a linear elastic orthotropic material model with the following properties (Table 3) is used.

Table 3 Engineering constants implemented in ABAQUS™.

E_{11} [MPa]	E_{22} [MPa]	E_{33} [MPa]	ν_{12} [-]	ν_{13} [-]	ν_{23} [-]	G_{12} [MPa]	G_{13} [MPa]	G_{23} [MPa]
56000	57000	5000	0.033	0.033	0.033	4175	4175	4175

The supports are meshed with a linear brick element with reduced integration, C3D8R; the mesh size is approximately 1 mm for both the rolls and the specimen.
To further reduce calculation time, a rigid-body constraint is enforced on the areas of the roll that do not make contact with the specimen. For these area's, ABAQUS™ assumes it is analytically rigid and does not calculate stresses nor strains.

As was previously mentioned, friction must also be modelled if the simulation is to be as realistic as possible. For the indenting roll, no tangential movement is expected. Therefore, a 'hard normal contact' is defined for this region.
For the supporting roll, there is a tangential movement, since the specimen slides over the roll as the displacement grows. In order to determine the friction coefficient, a number of simulations were performed, using different coefficients (Figure 13).
Since damage was not taken into account for these simulations, the calculated force should be an overestimation of the experimental force at higher displacements. Therefore, a coefficient between 0.2 and 0.3 is chosen. This also is in good agreement with the measurements done in [13]. For the ABAQUS™ friction formulation, a finite friction with a lagrange multiplier is chosen. With these conditions, an average simulation takes about six hours on the used computer.

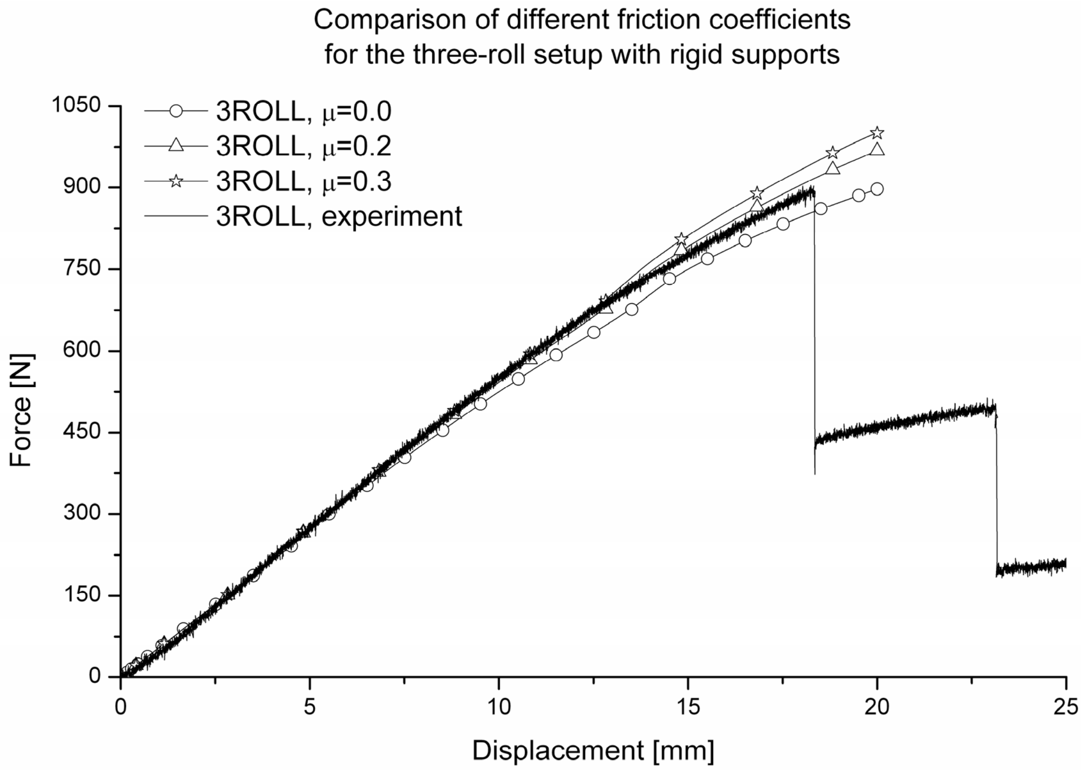

Figure 13 Comparison of the experiment with simulations using different friction coefficients for the three-point bending setup with rigid supports (3ROLL).

4.3. *Fully reversed three-point bending with rotating outer supports*

As in the previous paragraph, the setup is modelled using symmetry.
Since the central indenting rolls do not require any rotation, they are modelled by two separate rolls (Figure 14). To reduce calculation time, rigid body conditions are applied on all areas that do not contact the specimen. The element type is the same linear brick element with reduced integration, C3D8R, as before, the element size is 0.5 mm.

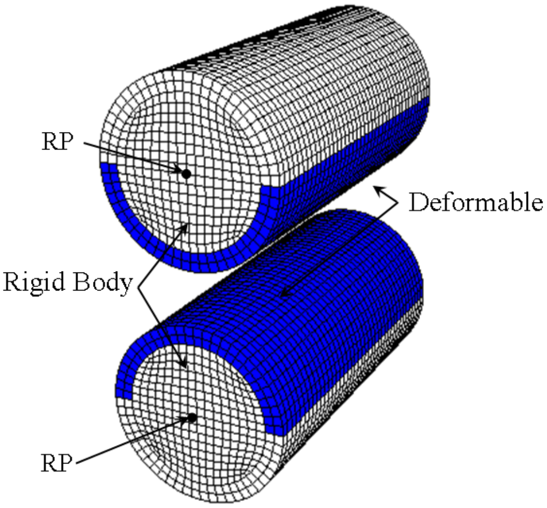

Figure 14 The model of the central indenter as two separate rolls.

The easiest way to model the rotating support is by modelling it as a single part, which is depicted in Figure 15. The rolls are slightly longer than the width of the specimen, so that the specimen does not make contact with the connecting part between the two rolls. Extra partitions are created (Figure 15 on the left) resulting in a better mesh. The distance between the two rolls is equal to the thickness of the specimen, the rolls have a diameter of 10, as was the case in the experimental setup.

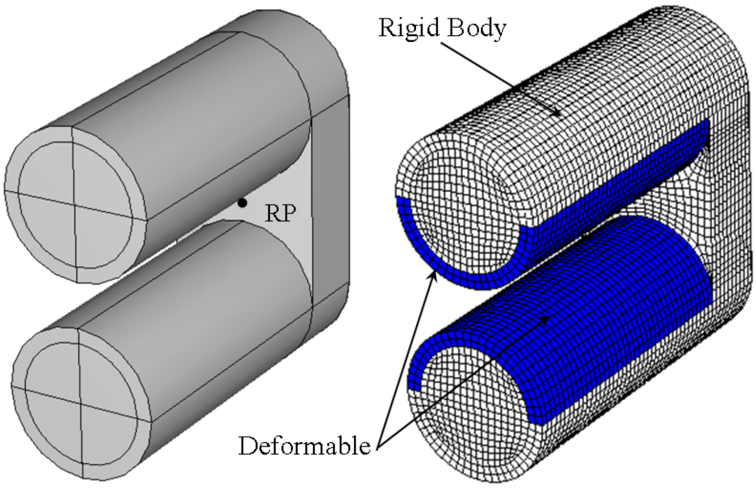

Figure 15 The model of the rotating support as one part.

Again there is a rigid-body constraint on all the partitions that do not make contact with the specimen, in order to save calculation time (Figure 15 on the right). The part is meshed with C3D8R elements; the element size is also 0.5 mm. The latter is done to assure that the calculation does not diverge as a result of contact problems.
For the boundary conditions of the rotating support, only the rotation of the support around its 'natural axis' is allowed, all other movement is constrained.
For the contact conditions, the slave surface is put on the support and the master surface is on the specimen. The latter helps the rotating of the support, since normally, the slave surface follows the movement of the master surface.
The symmetry conditions are the same as with the three-roll setup (Figure 16):
On plane A: $U_y = UR_x = UR_z = 0$
On plane B: $U_x = UR_y = UR_z = 0$

Of course, the symmetry conditions are also applied on the supports.
For the indenting support the boundary conditions are applied on both of the reference points. The movement along the x- and the y-axis is restricted and along the z-direction, a downward displacement of 20 mm is imposed.

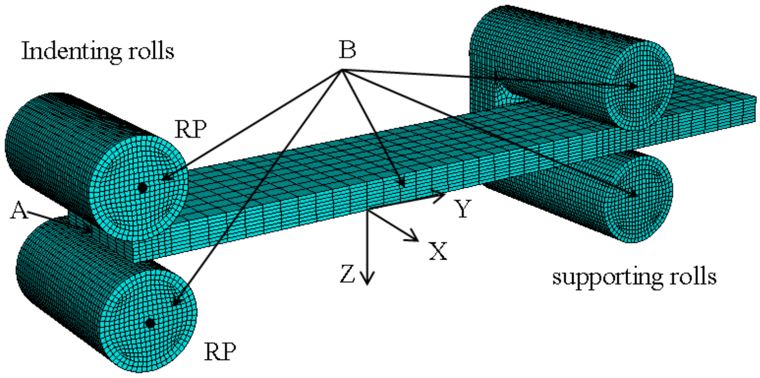

Figure 16 Illustration of the mesh and the boundary conditions for the three-point bending setup with rotating supports (6ROLL).

The specimen is a beam with dimensions 2.4 mm x 15 mm x 80 mm and it is meshed with quadratic brick element with reduced integration, C3D20R. The global size of the elements is 3 mm. However, in the zones of contact, the size is 1 mm to ensure that no convergence problems occur due to the contact conditions. The material model is the same as in the previous paragraph (see Table 3).
Friction is modelled in the same way as with the three-roll setup. Taking into account that damage was not modelled, a friction coefficient between 0.2 and 0.3 gives a good correspondence (Figure 17), although the correspondence is less than with the three-roll setup. No explanation could be found for the waviness of the simulation with μ equal to 0.2. Even with a denser mesh, it still occurred. Possibly it is the result of numerical instability due to the contact.

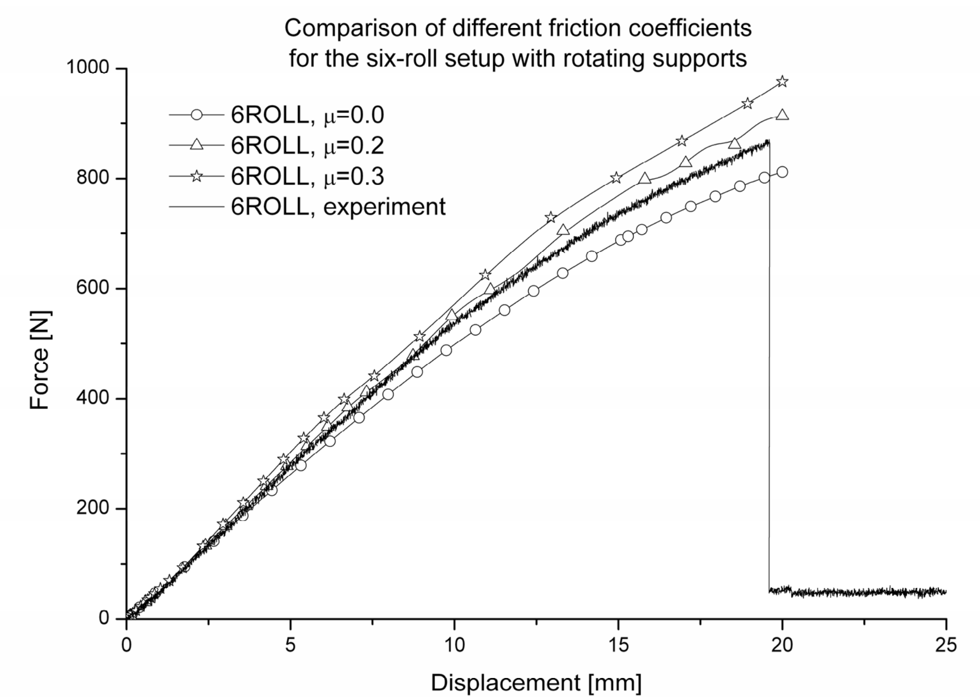

Figure 17 Comparison of the experiment with simulations using different friction coefficients for the fully reversed (6ROLL) setup.

In paragraph 3.1.1, it was mentioned that reason for the higher the bending stiffness and ultimate bending force for the single-sided setup lies in the setup. In Figure 18, it can clearly be seen that, for higher displacements, the necessary bending force for a given displacement is higher for the single-sided setup, for al implemented friction coefficients. As such, the influence of the used setup is proven.

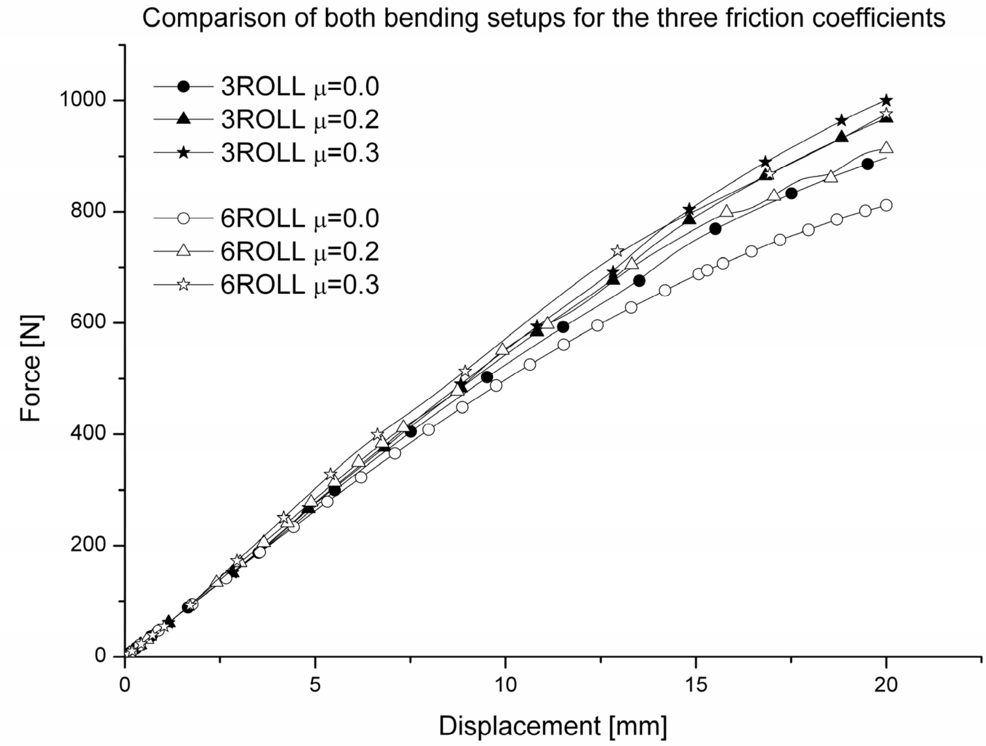

Figure 18 Illustration of the effect of the used bending setup on the bending stiffness and ultimate force.

This way of modelling leads to a converging calculation, but the calculation of the rotation of the support takes a lot of time. A simulation with a simple linear elastic orthotropic material model takes about thirty six hours to finish for a friction coefficient of 0.3. Adding a user-defined material model will only increase the time, so it is obvious that this model cannot be used for fatigue damage modelling, where multiple successive runs of this model are required.

In Figure 19, the calculated rotation of the support is plotted against a pseudo-time, where zero corresponds with the start of the simulation and one with the end. Two things can be noted: i) the effect whether the simulation is done frictionless ($\mu = 0.0$) or not, has a significant influence on the rotation and ii) if friction is modelled, the coefficient of friction does not have a large influence on the angle reached at the end of the simulation corresponding with a midspan displacement of 20 mm, nor on its evolution. The dip that occurs at the beginning (t=0.1) is a result of the numerical implementation of the contact. ABAQUS implicit requires a number of nodes to be connected numerically and as a result, the rotation of the support lags a little. This effect was also seen during the experiments, because there was a very small gap between the rolls and the specimen, to assure that no extra pressure was induced through the contact.

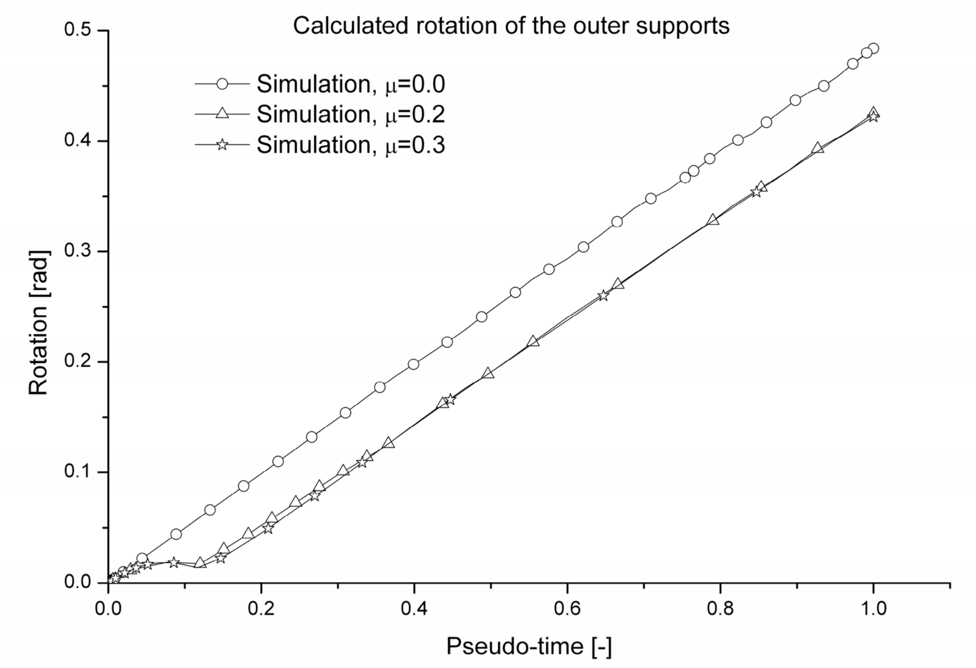

Figure 19 The rotation of the support as a function of the pseudo-time.

Now, the calculation is redone, but with a linear rotation added as a boundary condition on the reference point of the outer supports (Figure 15). As such, ABAQUS™ no longer needs to calculate the angle. The simulation was done for a friction coefficient of 0.2 and 0.3, with the corresponding final angles of 0.425 and 0.422 respectively (Figure 19). Under these circumstances, it only takes three hours and the corresponding force-displacement curve corresponds very well with the simulation with the normal boundary conditions (see Figure 20). However, it must be noted that for a given displacement, the force is a little larger than when the rotation is calculated, especially for the simulation with μ equal to 0.3.

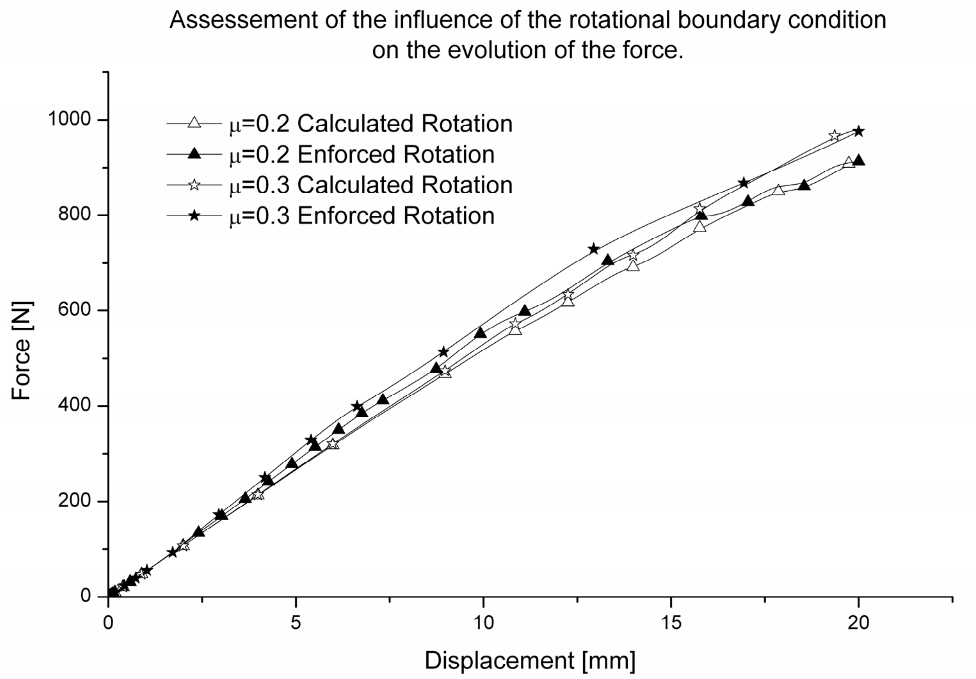

Figure 20 Comparison of the force-displacement curve for the simulations with different rotational boundary conditions.

As such, the computing time can be reduced drastically by enforcing the rotation on the outer supports, but unfortunately, it cannot be implemented for the validation of material models, since the angle of the rotational supports reached at full midspan displacement will depend on the stiffness of the specimen. Once damage occurs, this angle will change and the original boundary conditions will no longer be correct.

4.4. Results of the finite element simulations

It could already be noted that there is a very good correspondence in the evolution of the force as a function of the midspan displacement, both for the single sided (Figure 13) and the fully reversed bending setup (Figure 17).

The average midspan deflection at which fracture occurs for the single-sided setup, is about 17 mm (see Figure 10 and Figure 13). For this deflection, Figure 21 shows the longitudinal stresses for the simulation with μ equal to 0.2 which gave best correspondence in the force-displacement curve.

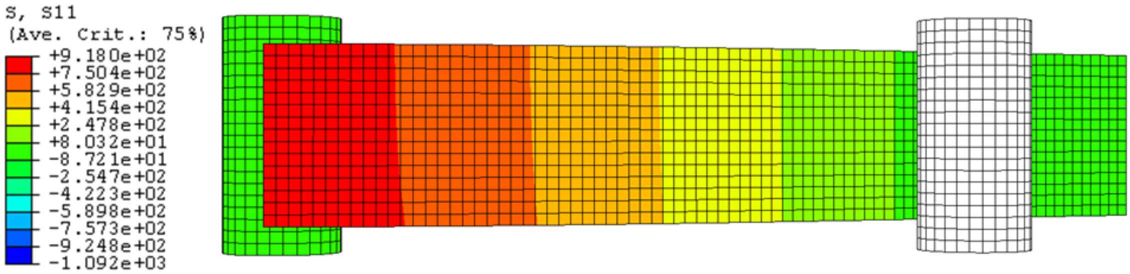

Figure 21 The longitudinal stress distribution (σ_{11}) at 17 mm midspan deflection for the single-sided setup.

It may be remarked that, despite the excellent agreement in the force-displacement curve (Figure 13), the longitudinal stresses are higher than the ultimate stress (Table 2). However, this simulation only includes linear elastic material behaviour. Implementing a damage model should only improve the agreement of both stresses and force-displacement curve.

The average midspan deflection at which fracture occurs for the fully reversed setup, is about 20 mm (see Figure 9). For this deflection, Figure 22 shows the stress along the fibres for the simulation with μ equal to 0.2. The bottom centre support has been removed for a better view on the stresses.

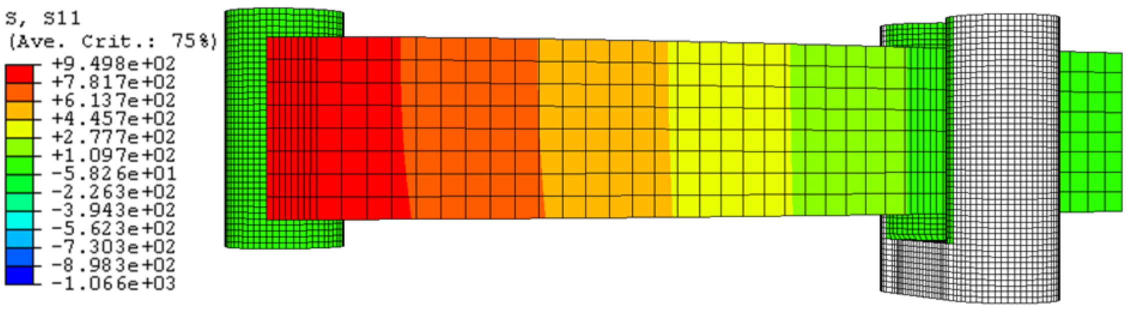

Figure 22 The longitudinal stress distribution (σ_{11}) at 20 mm midspan deflection for the fully reversed setup.

It can be noted that the occurring stresses in the centre of the specimen are again higher than the ultimate tensile strength (Table 2). This is due to the fact that no damage model was implemented.

5. Conclusions

In this study, the use of a three-point bending setup is considered as a setup for validating fatigue damage models for thin composite laminates with low bending stiffness. The loading conditions in three-point bending are quite interesting for this purpose, since they combine both tensile stresses on one side and compressive stresses on the other. Single-sided bending has the advantages of being easily modelled. The disadvantage of this setup is found in the experiments. After a few thousand cycles, the permanent deflection of the specimen causes the indenter to impact on the surface and therefore corrupting the fatigue data.

Fully reversed (symmetrical) bending does not have such a disadvantage. Furthermore, tension-compression fatigue is possible. However, the modelling in finite elements is problematic with long calculation times, due to the rotating of the supports.

Therefore, it may be concluded that despite of the interesting loading conditions of the setup, three-point bending in this configuration is not ideally suited for validating damage models for thin composite materials, because of the large midspan displacements which are reached.

Acknowledgements

The authors are highly indebted to the university research fund BOF (Bijzonder Onderzoeksfonds UGent) for sponsoring this research and to Ten Cate Advanced Composites, for supplying the composite material.

References

[1] Hansen, U. (1999). Damage development in woven fabric composites during tension-tension fatigue. Journal of Composite Materials, 33(7), 614-639.

[2] Coats, T.W. and Harris, C.E. (1995). Experimental verification of a progressive damage model for IM7/5260 laminates subjected to tension-tension fatigue. Journal of Composite Materials, 29(3), 280-305.

[3] Caprino, G. (2000). Predicting fatigue life of composite laminates subjected to tension-tension fatigue. Journal of Composite Materials, 34(16), 1334-1355.

[4] Gamstedt, E.K. and Sjogren, B.A. (1999). Micromechanisms in tension-compression fatigue of composite laminates containing transverse plies. Composites Science and Technology, 59(2), 167-178.

[5] Rotem, A. (1991). The fatigue behaviour of orthotropic laminates under tension-compression loading. International Journal of Fatigue, 13(3), 209-215.

[6] Sedrakian, A., Ben Zineb, T., Billoet, J.L., Sicot, N. and Lardeur, P. (1997). A numerical model of fatigue behaviour for composite plates: application to a three point bending test. In : Degallaix, S., Bathias, C. and Fougères, R. (eds.). International Conference on fatigue of composites. Proceedings, 3-5 June 1997, Paris, France, La Société Française de Métallurgie et de Matériaux, pp. 415-423.

[7] Sidoroff, F. and Subagio, B. (1987). Fatigue damage modelling of composite materials from bending tests. In : Matthews, F.L., Buskell, N.C.R., Hodgkinson, J.M. and Morton, J. (eds.). Sixth International Conference on Composite Materials (ICCM-VI) & Second European Conference on Composite Materials (ECCM-II) : Volume 4. Proceedings, 20-24 July 1987, London, UK, Elsevier, pp. 4.32-4.39.

[8] Caprino, G. and D'Amore, A. (1998). Flexural fatigue behaviour of random continuous-fibre-reinforced thermoplastic composites. Composites Science and Technology, 58, 957-965.

[9] I. De Baere, W. Van Paepegem, J. Degrieck, H. Sol , D. Van Hemelrijck and A. Petreli, Comparison of different identification techniques for measurement of quasi-zero Poisson's ratio of fabric reinforced laminates. Submitted to composites A

[10] Wim Van Paepegem, Mechanics of Materials, Faculty of Engineering, 2005

[11] Van Paepegem, W., De Geyter, K., Vanhooymissen, P. and Degrieck, J. (2006) Effect of friction on the hysteresis loops from three-point bending fatigue tests of fibre-reinforced composites. Composite Structures, Volume 72 issue 2, 212-217.

[12] K. De Geyter and P. Vanhooymissen, Internal report on fatigue of carbonfibre-reinforced thermoplastics, Faculty of Engineering, Ghent University

[13] Quintelier J, Samyn P, De Baets P, Tuzolana T, Van Paepegem W, Van den Abeele F, Vermeulen J, Wear behaviour of carbon fibre-reinforced poly(phenylene sulphide), POLYMER COMPOSITES 27 (1): 92-98, FEB 2006